



Published in final edited form as:

*Environ Sci Technol.* 2009 August 1; 43(15): 5921–5927.

## Transverse bacterial migration induced by chemotaxis in a packed column with structured physical heterogeneity

Meng Wang and Roseanne M. Ford\*

Department of Chemical Engineering, University of Virginia, Charlottesville, VA 22904

### Abstract

The significance of chemotaxis in directing bacterial migration towards contaminants in natural porous media was investigated under groundwater flow conditions. A laboratory-scale column, with a coarse-grained sand core surrounded by a fine-grained annulus, was used to simulate natural aquifers with strata of different hydraulic conductivities. A chemoattractant source was placed along the central axis of the column to model contaminants trapped in the heterogeneous subsurface. Chemotactic bacterial strains, *Escherichia coli* HCB1 and *Pseudomonas putida* F1, introduced into the column by a pulse injection, were found to alter their transport behaviors under the influence of the attractant chemical emanating from the central source. For *E. coli* HCB1, approximately 18% more of the total population relative to the control without attractant exited the column from the coarse sand layer due to the chemotactic effects of  $\alpha$ -methylaspartate under an average fluid velocity of 5.1 m/d. Although *P. putida* F1 demonstrated no observable changes in migration pathways with the model contaminant acetate under the same flow rate, when the flow rate was reduced to 1.9 m/d, approximately 6–10% of the population relative to the control migrated from the fine sand layer towards attractant into the coarse sand layer. Microbial transport properties were further quantified by a mathematical model to examine the significance of bacterial motility and chemotaxis under different hydrodynamic conditions, which suggested important considerations for strain selection and practical operation of bioremediation schemes.

### Keywords

porous media; chemotaxis; heterogeneity; transport; bacteria

## INTRODUCTION

In recent years, bioremediation has become a viable option in the restoration of contaminated aquifers (1,2). However, the process is technologically challenging because of the difficulty in delivering the microbial populations to the target locations. Groundwater flow usually drives bacteria to transport through highly conductive regions of the subsurface, leaving the pollutants trapped within low permeable zones without treatment (3,4). Chemotaxis, the ability of bacteria

\*Corresponding author phone: (434) 924-6283; fax: (434) 982-2658; rmf3f@virginia.edu. Department of Chemical Engineering, University of Virginia, 102 Engineers' Way, P.O. Box 400471, Charlottesville, VA 22904-4741.

### SUPPORTING INFORMATION AVAILABLE

Tracer tests in different types of heterogeneous columns to correlate the double-peak breakthrough configurations and column structures are provided in Figures S1–S2; homogeneous column studies to compare the transport properties between *E. coli* and *P. putida* are given in Figures S3–S4 and the agarous plug assays to demonstrate the chemotactic responses of tested strain-attractant pairs are presented in Figure S5.

### BRIEF

A structured heterogeneous column study revealed the significant role of chemotaxis in directing transverse microbial migration in natural porous media.

to sense chemical gradients and migrate preferentially toward regions with high chemoattractant concentrations, is considered to enhance bioremediation by directing microorganisms towards closer contact with the residual contaminants in less conductive zones in aquifers (5–8).

Chemotaxis in aqueous systems has been well demonstrated and characterized (9–11). Individual bacterial swimming behavior in isotropic solutions is characterized as a three-dimensional random walk. As a chemotactic microorganism swims up attractant gradients, the frequency of cell body reorientation decreases and the swimming length interval increases (12), resulting in a net migration of the microbial population towards higher chemical concentrations. It was also observed that bacterial chemotaxis was not suppressed by convective flow and could still concentrate biomass within chemical gradients transverse to flow (13).

In contrast, chemotaxis in porous media was more recently identified and documented. Pedit and coworkers (14) used a capillary filled with glass beads and indicated that the accumulation of *Pseudomonas putida* G7 was higher in the capillaries initially containing naphthalene than in the no-attractant controls. A statistically significant chemotactic response was reported by Olson et al. (15), who noted a chemotactic band of *Pseudomonas putida* F1 to toluene in a column containing glass-coated polystyrene beads using Sherwood et al.'s (16) magnetic resonance imaging method. Roush et al. (17) suggested that chemotaxis was enhanced in a heterogeneous medium by examining swarm plates with a rectangular shaped sand-filled area. Wang et al.'s study (18) with a static heterogeneous filter-chamber indicated that *Pseudomonas putida* F1 was attracted to higher contaminant concentrations and this trend was augmented by the associated microbial growth on the contaminant. Long and Ford (19) fabricated a two-dimensional microfluidic device with a homogeneous porous media matrix and reported a strong chemotactic bacterial migration up the attractant gradients transverse to the flow.

Previous chemotaxis studies in porous media were generally conducted either under static or homogeneous conditions or in artificial porous media. However, the complexity and heterogeneity of natural aquifers introduce a number of differences and uncertainties compared to the artificial laboratory conditions. It is therefore important to gain a quantitative understanding of the significance of chemotaxis in a natural heterogeneous system when the other transport processes such as advection, dispersion, adsorption and retardation occur. In this study, a saturated, intermediate-scale laboratory column, comprised of two layers of quartz sand with contrasting conductivities, was used to mimic the heterogeneous subsurface. Our objective was to use this controlled system with well-characterized heterogeneities to investigate the effectiveness and magnitude of the chemotactic influence on bacterial transport properties in order to improve our understanding of the chemotactic impact occurring in *in situ* bioremediation processes.

## EXPERIMENTAL SECTION

### Bacteria and Attractant Systems

The structured-column transport experiments were performed by testing two bacterial strains: *Escherichia coli* HCB1 (20) and *Pseudomonas putida* F1 (21). *E. coli* HCB1 demonstrates a strong chemotactic response to  $\alpha$ -methylaspartate ( $\alpha$ -mASP, Sigma-Aldrich) (13), a non-metabolizable analog of aspartate. The chemical was initially dissolved in pre-heated 3% low melting agarose (NuSieve GTG Agarose, FMC Bioproducts) solution to obtain a final concentration of 0.1 mM to serve as the attractant source. An equivalent amount of sodium chloride was used during the control experiments without attractant to maintain the same ionic strength. The other tested strain and attractant pair was *P. putida* F1 and sodium acetate. *P. putida* F1 was chosen because of its chemotaxis to and catabolism of various recalcitrant

pollutants (22). Its mutant *P. putida* F1 CheA (23) maintained all the wild-type's properties except its chemotactic ability, which therefore served as the nonchemotactic control.

*E. coli* HCB1 was cultured in 50 mL of growth media comprised of 50% Luria Broth (Fisher) media and 50% Modified Hunter's Mineral Base (MSB) in a sterile 250 mL baffled shake flask. It took the bacteria ~10 hours to reach its mid-exponential growth at O.D. (590nm) = 1.0 (Beckman, DU-7) in a LabLine Environ-shaker (model 3528-5) at 150 rpm and 27 °C. *P. putida* F1 and its mutant reached mid-exponential growth in ~20 h in MSB media augmented with 5 mM acetate under the same culture conditions. Bacteria cultures were then filtered on a 0.22 µm filter (Millipore GSWP14250) and resuspended in a 10 mM nitrate solution to reach the final concentration of  $\sim 7 \times 10^8$  cells/mL for *E. coli* and  $\sim 3 \times 10^9$  cells/mL for *P. putida*. Additionally, fluorescent microspheres (Microgenics Corporation, R0100) with a diameter of 1 µm were washed with DI water and resuspended in *P. putida* injectates to obtain a final concentration of  $\sim 1 \times 10^9$  particles/mL. Because of its similar size to *P. putida*, the microsphere served as an immobile particle tracer (24). All bacteria were observed to swim vigorously at 40× using a Zeiss Std 16 microscope to visually confirm their motility prior to injection.

### Column Assembly

To simulate layers of porous media with different conductivities, coarse- and fine- grained sand, with mean grain sizes of 710 µm (VWR, 20117-088) and 450 µm (VWR, 20118-003) respectively, were wet-packed into a glass chromatography column (diameter 4.8 cm, length 15.5 cm) with a structure similar to Saiers et al. (25) and Morley et al. (26) as shown in Fig. 1a. Quartz sands were washed with 10% (v/v) hydrochloric acid and then 0.5 M NaOH. After rinsed thoroughly with de-ionized water, they were dried in an Isotemp Oven (Fisher) at 80 °C. The attractant source was made by pouring attractant-containing, pre-heated agarose solution into a hollow column made by plastic nylon mesh (190 µm opening, McMaster-Carr), which was originally inserted into a rigid straw (diameter: 0.475 cm) to maintain its cylindrical shape. The layered structure of the column was achieved by packing fine-grained sand in the annulus surrounding a center tube (diameter 1.8 cm) and pouring coarse-grained sand in the tube after placing the rigid straw along the central axis line. Then the center tube and the straw were removed gently. This procedure produced a central core of coarse material with a centerline attractant source, running parallel to the flow, and a surrounding annulus of fine material (Fig. 1a). An attractant gradient formed in the transverse direction as attractant diffused from the agar core, spreading across both coarse and fine media under flow (Fig. 1b).

### Transport Experiments and Sample Analysis

A variable-flow peristaltic pump (Fisher, 13-876-1) was used to maintain a constant head through the column to yield an average flow velocity of 5.1 m/d. A syringe pump (KD Scientific 230) was applied to the system to produce a lower flow rate of 1.9 m/d. Because of the contrasting hydraulic conductivities of the media (Fig. 1c), the coarse sand core was a flow path with a higher average velocity ( $V_1$ ) than the velocity in the fine annulus ( $V_2$ ). After a stabilization period of 0.2 pore volume, a 2 mL injectate was introduced in the column by a three-way valve and a syringe pump (Harvard PHD 2000). Samples were manually collected at the column outlet approximately every 3 minutes over a total time of 90 minutes for the fast flow rate and every 8 minutes over a period of 4 hours for the slow flow rate.

One portion of the sample (~2 mL) was filtered by a 0.45 µm nylon syringe filter (Fisher, 097206) immediately after collection to remove any colloids. The filtered solution was then measured at 220 nm to obtain nitrate concentration (Beckman, DU-640). The remaining sample was preserved with 37% formaldehyde (Fisher) to reach 10% v/v and stored in 4 °C refrigerator. The microbial population in the preserved sample, measured no later than 12 hours after it was collected, was enumerated using the Acridine Orange counting method (27). The concentration

of fluorescent beads was determined from the same slide using a UV-fluorescent microscope (Zeiss Ph3 F100/1.25 Oil, 160/-). For each experiment, replicates were performed and data points from all replicates are included in the figure plots.

### Mathematical model

A one-dimensional bacterial conservation equation was applied to quantify the chemotactic influence on the observed bacterial migration (28):

$$R \frac{\partial b}{\partial t} + k_m b = D_{bz} \left( \frac{\partial^2 b}{\partial z^2} \right) - V_f \frac{\partial b}{\partial z} \quad (1)$$

where  $b$  (cells/mL) represents the bacterial concentration in aqueous phase,  $R$  represents the bacterial retardation coefficient in porous media and  $V_f$  (m/d) represents the interstitial linear fluid velocity. The longitudinal dispersion coefficient  $D_{bz}$  (cm<sup>2</sup>/s) was defined as (16):

$$D_{bz} = \frac{\mu_{0,\text{eff}}}{\varepsilon} + \alpha_z V_f \quad (2)$$

in which  $\alpha_z$  (cm) is the longitudinal dispersivity,  $\varepsilon$  is the porosity, and  $\mu_{0,\text{eff}}$  (cm<sup>2</sup>/s) is the effective bacterial motility coefficient which is related to the bacterial random motility coefficient  $\mu_0$  (cm<sup>2</sup>/s) in the bulk liquid phase and the tortuosity  $\tau$  by:

$$\frac{\mu_{0,\text{eff}}}{\varepsilon} = \frac{\mu_0}{\tau} \quad (3)$$

The linear term proportional to bacterial concentration,  $k_m b$  (cells/mL·h<sup>-1</sup>), was used to quantify the change in bacterial mass due to retention and chemotaxis within each porous media layer (29).

This mathematical model was solved numerically by a finite-difference method using a MATLAB code. Different groups of parameter values were obtained by fitting the model to the data in each conductive layer.

## RESULTS AND DISCUSSION

### Hydrodynamics in a structured column with bimodal conductivity

The pulse injection experiment with nitrate tracer provided information about the flow patterns in the structured column (Supporting Information Part I). Due to the bimodal conductivity of the structured column, the fixed pressure head maintained at the column ends established a nonuniform flow field; the total flux was diverted into two main components, one with a higher velocity in the coarse sand core and the other one with a lower velocity in the fine sand annulus. This heterogeneous flow condition produced a breakthrough curve (BTC) with double peaks for an injected pulse as indicated in Fig 2, under the flow rate of 5.1 m/d. BTCs at the lower flow rates were similar. The first peak of the curve appeared earlier than 1 pore volume and represented the mass transporting through the conductive coarse sand core while the second peak accounted for mass from the low permeable fine sand annulus. The saddle between two peaks indicated solute transport in the mixing zone at the interface between two layers, which was a result of the mass dispersion from the adjacent two flow layers and also included the directed migration across the interface due to chemotaxis in the bacterial experiments.

### ***E. coli* HCB1 Transport with Chemotaxis**

*E. coli* HCB1 BTCs were collected and compared to the controls without attractant. As indicated by the data plotted in Fig. 3, an apparent mass increase was observed in the first peak and an associated mass decrease was detected in the second peak for the chemotactic bacterial BTCs relative to the control ones. The microbial recoveries associated with the two peaks changed from  $36.7 \pm 2.2\%$  and  $45.9 \pm 4.3\%$  to  $54.2 \pm 1.5\%$  and  $28.6 \pm 1.7\%$  when the attractant source was present. This significant mass shift between peaks implied that a larger portion of the chemotactic bacteria migrated through the conductive core due to the attractant gradients in the radial direction transverse to flow. In response to a higher chemoattractant level, microorganisms which originally entered the low permeable annulus swam across the interface to the inner high velocity region, leading to the changes in the bacterial recoveries exiting from the two layers.

### ***P. putida* F1 Transport at Two Different Flow Rates**

The transport studies in the structured column for the strain *P. putida* F1 and its nonchemotactic mutant were performed initially under the same flow rate as *E. coli* HCB1. As shown in Fig. 4, the bacteria exhibited nearly the same characteristics in the BTCs as the nonmotile microspheres. Similar bacterial distributions were observed for both chemotaxis and control cases at two initial acetate concentrations (0.1 mM and 1 mM). No chemotactic response was detected under this high flow rate. However, when the average fluid velocity was reduced to 1.9 m/d, the mass recovery of the first peak was increased from  $35.3 \pm 0.7\%$  to  $41.8 \pm 2.2\%$  and that of the second peak was reduced from  $31.3 \pm 4.9\%$  to  $22.8 \pm 2.8\%$  in *P. putida*'s BTCs compared to the nonchemotactic mutants as illustrated in Fig. 5. Unlike *E. coli*'s breakthroughs, the configuration of all curves for *P. putida* and microspheres had a relatively higher first peak and a lower second one, which was largely due to the microbe's preferable adsorption to fine sand (Supporting Information: Part II). Under the low flow rate, which is more comparable to that of natural aquifers, the observable changes in the chemotactic *P. putida* BTCs were attributed to the directed bacterial migration between two adjacent permeable regions towards the attractant source, as in the *E. coli* experiments.

The biased bacterial distribution in the bimodal conductive system as indicated in both Fig. 3 and Fig. 5 provided strong evidence of bacterial chemotaxis in a porous medium flow field. The results revealed the significance of chemotaxis in affecting the macroscopic bacterial transport in a heterogeneous porous medium with characteristics reflecting those relevant to the natural environment, especially under low flow rate conditions. Moreover, our results indicated the importance of bacterial motility when the flow rate was low enough to become comparable to the microbial swimming velocity. The apparent lower recovery of nonmotile particles compared to microorganisms from the fine sand layer in the control experiment (Fig. 5b) clearly demonstrated that self-motility enabled bacteria to transport more efficiently in the low permeable zones at low flow rate conditions, as reported previously by Camesano and Logan (30). Other factors that may affect the microbial counts measured in effluent samples such as bacterial growth, decay and changes in swimming behaviors during the transport process were expected to be the same for the chemotactic experiments and the controls, although we did not directly measure these.

Experimental evidence in the study of *P. putida* revealed the importance of hydrodynamic effects on chemotaxis observed in the structured column. A slower flow rate likely allowed the attractant to be transported further in transverse direction thus exposing a greater proportion of the microbial population to the attractant, and ultimately resulting in a greater overall chemotactic response. Sen et al. (31)'s computational result, which simulated the situation combining both convection and chemotaxis in homogeneous porous media, supported the explanation that chemotaxis had a significant effect on bacterial transport at low pore velocity.



Furthermore, a lower flow rate yielded a lower fluid velocity and lower shear rate across pore spaces, resulting in a lower impact on the microscopic microbial swimming patterns in the porous matrix.

The chemotactic response of bacteria within the structured columns was consistent with observations reported previously. Lanning and coworkers (13) noted that the chemotactic response of *E. coli* toward  $\alpha$ -mASP was not impeded in the transverse direction when the average flow rate increased from 9.5 m/d to 95.0 m/d in an aqueous solution. However, within a shear flow field which occurs in narrow pore spaces, Marcos and Stocker (32) observed that microbial swimming trajectories followed fluid streamlines rather than independent trajectories at high shear rates. Therefore, in column experiments for *P. putida* at a high flow rate, it was likely that bacterial swimming was constrained by the local fluid velocity and shear stress within the pore spaces to the extent that a chemotactic response was not detected.

The chemotactic response of bacteria may also influence their interaction with the solid surfaces of the packed columns (33). Velasco-Casal et al. (34) noted a reduced deposition of *P. putida* G7 on the grain surface in the presence of the chemoattractant naphthalene. In our study, such a reduction in bacterial retention caused by chemotaxis was consistent with a higher chemotactic bacterial recovery in the coarse sand layer. However, because the decrease of the second peak in the bacterial BTCs occurred simultaneously, the preferable bacterial migration across the layer's interface driven by chemotaxis was still recognized as the dominant reason for the difference between chemotactic and control bacterial BTCs.

The distinct transport behaviors between *E. coli* and *P. putida* under different hydrodynamic conditions may be attributed in part to the difference in their microscopic swimming properties and the strength of their chemotactic response. *E. coli* HCB1 was reported to have a mean swimming speed of 22.8  $\mu\text{m/s}$  ( $\sim 2.0$  m/d) and a motility coefficient of  $3.3 \times 10^{-6} \text{ cm}^2/\text{s}$  (35) while reported values for *P. putida* were 44  $\mu\text{m/s}$  ( $\sim 4$  m/d) and  $13 \times 10^{-6} \text{ cm}^2/\text{s}$ , respectively (21). In contrast to the tumbling motion between successive swimming trajectories of *E. coli*, *P. putida* exhibits primarily a forward and backward motion. In small diameter sediment pores, the faster swimming speed and longer run lengths between reorientations of *P. putida* result in more encounters with the solid surface of the porous medium, which may inhibit motility. For example, it was reported that the motility coefficient of *P. putida* F1 in a 250  $\mu\text{m}$ -diameter glass-coated polystyrene bead pack ( $0.15 \times 10^{-6} \text{ cm}^2/\text{s}$ ) was significantly less than that for *E. coli* ( $0.50 \times 10^{-6} \text{ cm}^2/\text{s}$ ) (15). The difference in the strength of the chemotactic response may also contribute to the observed differences in BTCs between the two microorganisms. The chemotactic sensitivity coefficient, one parameter to quantify the magnitude of chemotaxis, was reported as  $2.4\text{--}4.1 \times 10^{-4} \text{ cm}^2/\text{s}$  for *E. coli*'s response to  $\alpha$ -mASP (35,36) and  $0.18\text{--}2.9 \times 10^{-4} \text{ cm}^2/\text{s}$  for *P. putida*'s response to naphthalene (14,37). Additional experimental support to demonstrate the higher sensitivity of the strain-attractant pair of *E. coli* compared to *P. putida* used in our study is presented in Supporting Information (Part III).

### Quantification by Mathematical Models

Fitted curves from the one-dimensional model are plotted along with the experimental data in Fig. 2, Fig. 3 and Fig. 5. The double-peak configuration was obtained by superimposing two independent single peak curves, each representing the mass transport in one layer. The values of fitted parameters in Table 1 were determined by minimizing the root mean squared error between experimental data and simulated results. Because transport in the mixing zone was neglected, the simulated results underestimated bacterial concentration in the intermediate part of the curve; however, the model successfully predicted the two peaks where significant variations in BTCs were observed.

Based on the agreement between the mathematical model and experimental data, the hypothesis of two differing flow layers in the experimental system was supported. The average flow velocity in each zone was calculated according to the breakthrough time of each peak. The peak's width was controlled by longitudinal dispersion and its height was an indicator of the mass variation in the fluid phase over the entire experimental period, which was quantified by the  $k_m$  value. The significant decrease of  $k_m$  in the fast flow layer and the corresponding increase in the slow flow layer in chemotaxis tests reflected the strong impact of the chemoattractants for both microorganisms. The height of the first peak in the *E. coli* chemotactic BTC was 1.5-fold higher than the control, representing approximately 18% more of the total population exiting from the coarse sand layer. This response was reflected by a decrease in the  $k_m$  value from  $1.2 \text{ h}^{-1}$  (control) to  $-0.2 \text{ h}^{-1}$  (chemotaxis). The negative sign indicates that the apparent bacterial recovery in the fast flow layer was even larger than the tracer; this was attributed to bacterial migration from the adjacent slow flow layer due to chemotaxis. The value of  $D_{bz}$  in the coarse sand layer for the chemotactic BTCs was smaller than the controls, which might be because the chemotactic effect reduced the dispersal of bacteria by concentrating the population near the higher attractant level of the inner source. For fluid velocity in the range from 3 to 8 m/d, the value of  $\alpha_z$  for the bacteria was similar to the tracer's but was an order of magnitude higher when the fluid velocity was 1 m/d, during which the bacterial motility contributed significantly to the population's transport as reported previously (30,38–40). The same simulated microsphere BTC in Fig. 5a and 5b indicated consistency of the nonmotile particle transport in the chemotaxis and control experiments.

### Implications for Bioremediation

This study demonstrated the potential advantages of chemotactic bacteria to facilitate access to pollutants trapped in heterogeneous aquifers in order to enhance bioremediation efficiency. In natural systems, contaminants may serve as nutrients as well as chemoattractants, which will further augment the difference in the microbial distribution between strains with and without chemotaxis by stimulating biomass growth in the zones near the chemical source. Consequently, contaminant clean-up rates could be highly accelerated due to the greater availability of contaminant-degrading bacteria that exhibit chemotactic migration. Therefore, it may be beneficial to consider chemotaxis and motility in addition to degradation capabilities as criteria for bacterial strain selection in bioremediation. As suggested by the distinct transport behaviors of *E. coli* and *P. putida*, bioremediation schemes should be adjusted to take advantage of microbial specific swimming characteristics; natural-gradient implementation may be preferable to forced-gradient when transport of the injected strain is extremely restricted in porous media, and moderate circulation might be applied to the site when microorganisms with strong chemotactic ability are used to enhance process efficiency.

### Supplementary Material

Refer to Web version on PubMed Central for supplementary material.

### ACKNOWLEDGMENT

The authors gratefully acknowledge David Metge and Dr. Ronald W. Harvey for providing instruments for and assistance with the preliminary column tests at the U.S. Geological Survey in Boulder, CO. Laura Brashear's editorial assistance with the manuscript was greatly appreciated. Acknowledgment is made to the Donors of the American Chemical Society Petroleum Research Fund (ACS-PRF 38031-AC9) for partial support of this research. This work was also funded by the National Science Foundation (EAR 0408454) and a fellowship from the NIH Biotechnology Training Program at the University of Virginia.

## REFERENCES

1. Gibert O, Ferguson AS, Kalin RM, Doherty R, Dickson KW, McGeough KL, Robinson J, Thomas R. Performance of a sequential reactive barrier for bioremediation of coal tar contaminated groundwater. *Environ. Sci. Technol* 2007;41:6795–6801. [PubMed: 17969697]
2. Steffan RJ, Sperry KL, Walsh MT, Vainberg S, Condee CW. Field-scale evaluation of in situ bioaugmentation for remediation of chlorinated solvents in groundwater. *Environ. Sci. Technol* 1999;33:2771–2781.
3. Gierczak RFD, Devlin JF, Rudolph DL. Combined use of field and laboratory testing to predict preferred flow paths in an heterogeneous aquifer. *J. Contam. Hydrol* 2006;82:75–98. [PubMed: 16246459]
4. Lee M, Saunders JA, Wolf LW. Effects of geologic heterogeneities on pump-and-treat and In situ bioremediation: A stochastic analysis. *Environ. Eng. Sci* 2000;17:183–189.
5. Marx RB, Aitken MD. Bacterial chemotaxis enhances naphthalene degradation in a heterogeneous aqueous system. *Environ. Sci. Technol* 2000;34:3379–3383.
6. Grimm A, Harwood C. Chemotaxis of *Pseudomonas* spp. to the polyaromatic hydrocarbon naphthalene. *Appl. Environ. Microbiol* 1997;63:4111–4115. [PubMed: 9327579]
7. Long W, Hilpert M. Lattice-Boltzmann modeling of contaminant degradation by chemotactic bacteria: Exploring the formation and movement of bacterial bands. *Water Resour. Res* 2008;44:15.
8. Parales RE, Haddock JD. Biocatalytic degradation of pollutants. *Curr. Opin. Biotechnol* 2004;15:374–379. [PubMed: 15296933]
9. Mesibov R, Ordal GW, Adler J. The range of attractant concentrations for bacterial chemotaxis and the threshold and size of response over this range: Weber law and related phenomena. *J. Gen. Physiol* 1973;62:203–223. [PubMed: 4578974]
10. Ford RM, Phillips BR, Quinn JA, Douglas AL. Measurement of bacterial random motility and chemotaxis coefficients: I. Stopped-flow diffusion chamber assay. *Biotechnol. Bioeng* 1991;37:647–660. [PubMed: 18600656]
11. Tindall M, Maini P, Porter J, Armitage JP. Overview of mathematical approaches used to model bacterial chemotaxis II: bacterial populations. *Bull. Math. Biol* 2008;70:1570–1607. [PubMed: 18642047]
12. Berg HC, Brown DA. Chemotaxis in *Escherichia coli* analysed by Three-dimensional Tracking. *Nature* 1972;239:500–504. [PubMed: 4563019]
13. Lanning LM, Ford RM, Long T. Bacterial chemotaxis transverse to axial flow in a microfluidic channel. *Biotechnol. Bioeng* 2008;100:653–663. [PubMed: 18306417]
14. Pedit JA, Marx RB, Miller CT, Aitken MD. Quantitative analysis of experiments on bacterial chemotaxis to naphthalene. *Biotechnol. Bioeng* 2002;78:626–634. [PubMed: 11992528]
15. Olson MS, Ford RM, Smith JA, Fernandez EJ. Quantification of bacterial chemotaxis in porous media using magnetic resonance imaging. *Environ. Sci. Technol* 2004;38:3864–3870. [PubMed: 15298194]
16. Sherwood JL, Sung JC, Ford RM, Fernandez EJ, Maneval JE, Smith JA. Analysis of Bacterial Random Motility in a Porous Medium Using Magnetic Resonance Imaging and Immunomagnetic Labeling. *Environ. Sci. Technol* 2003;37:781–785. [PubMed: 12636279]
17. Roush C, Lastoskie C, Worden R. Denitrification and chemotaxis of *Pseudomonas stutzeri* KC in porous media. *J. Environ. Sci. Health., Part A* 2006;41:967–983.
18. Wang M, Ford RM, Harvey RW. Coupled effect of chemotaxis and growth on microbial distributions in organic-amended aquifer sediments: Observations from laboratory and field studies. *Environ. Sci. Technol* 2008;42:3556–3562. [PubMed: 18546689]
19. Long T, Ford RM. Enhanced transverse migration of bacteria by chemotaxis in a porous T-sensor. *Environ. Sci. Technol.* 2009(Accepted)
20. Wolfe, AJ.; Conley, MP.; Kramer, TJ.; Berg, HC. Vol. Vol. 169. 1987. Reconstitution of signaling in bacterial chemotaxis; p. 1878-1885. In
21. Harwood CS, Fosnaugh K, Dispensa M. Flagellation of *Pseudomonas putida* and analysis of its motile behavior. *J. Bacteriol* 1989;171:4063–4066. [PubMed: 2738028]



22. Parales RE, Ditty JL, Harwood CS. Toluene-degrading bacteria are chemotactic towards the environmental pollutants benzene, toluene, and trichloroethylene. *Appl. Environ. Microbiol* 2000;66:4098–4104. [PubMed: 10966434]
23. Liu X, Wood PL, Parales JV, Parales RE. Chemotaxis to Pyrimidines and Identification of a Cytosine Chemoreceptor in *Pseudomonas putida*. *Journal of Bacteriology* 2009;191:2909–2916. [PubMed: 19251854]
24. Harvey RW, Kinner NE, Bunn A, MacDonald D, Metge D. Transport behavior of groundwater protozoa and protozoan-sized microspheres in sandy aquifer sediments. *Appl. Environ. Microbiol* 1995;61:209–217. [PubMed: 16534904]
25. Sayers JE, Hornberger GM, Harvey C. Colloidal silica transport through structured, heterogeneous porous media. *J. Hydrol* 1994;163:271–288.
26. Morley LM, Hornberger GM, Mills AL, Herman JS. Effects of transverse mixing on transport of bacteria through heterogeneous porous media. *Water Resour. Res* 1998;34:1901–1908.
27. Hobbie JE, Daley RJ, Jasper S. Use of nuclepore filters for counting bacteria by fluorescence microscopy. *Appl. Environ. Microbiol* 1977;33:1225–1228. [PubMed: 327932]
28. Tufenkji N. Modeling microbial transport in porous media: Traditional approaches and recent developments. *Adv. Water Res* 2007;30:1455–1469.
29. Tufenkji N, Redman JA, Elimelech M. Interpreting deposition patterns of microbial particles in laboratory-scale column experiments. *Environ. Sci. Technol* 2003;37:616–623. [PubMed: 12630480]
30. Camesano TA, Logan BE. Influence of fluid velocity and cell concentration on the transport of motile and nonmotile bacteria in porous media. *Environ. Sci. Technol* 1998;32:1699–1708.
31. Sen TK, Das D, Khilar KC, Suraishkumar GK. Bacterial transport in porous media: New aspects of the mathematical model. *Colloids Surf. A* 2005;260:53–62.
32. Marcos, Stocker R. Microorganisms in vortices: a microfluidic setup *Limnol. Oceanogr. Methods* 2006;4:392–398.
33. Nelson KE, Ginn TR. Theoretical investigation of bacterial chemotaxis in porous media. *Langmuir* 2001;17:5636–5645.
34. Velasco-Casal P, Wick LY, Ortega-Calvo J-J. Chemoeffectors decrease the deposition of chemotactic bacteria during transport in porous media. *Environ. Sci. Technol* 2008;42:1131–1137. [PubMed: 18351083]
35. Lewus P, Ford RM. Quantification of random motility and chemotaxis bacterial transport coefficients using individual-cell and population-scale assays. *Biotechnol. Bioeng* 2001;75:292–304. [PubMed: 11590602]
36. Strauss I, Frymier P, Hahn C, Ford RM. Analysis of bacterial migration. II. Studies of multiple attractant gradients. *AICHE J* 1995;41:402–414.
37. Marx RB, Aitken MD. Quantification of chemotaxis to naphthalene by *Pseudomonas putida* G7. *Appl. Environ. Microbiol* 1999;65:2847–2852. [PubMed: 10388674]
38. Camper A, Hayes J, Sturman P, Jones W, Cunningham AB. Effects of motility and adsorption rate coefficient on transport of bacteria through saturated porous media. *Appl. Environ. Microbiol* 1993;59:3455–3462. [PubMed: 16349075]
39. Becker MW, Metge D, Collins SA, Shapiro AM, Harvey RW. Bacterial transport experiments in fractured crystalline bedrock. *Ground Water* 2003;41:682–689. [PubMed: 13678122]
40. Becker MW, Collins SA, Metge DW, Harvey RW, Shapiro AM. Effect of cell physicochemical characteristics and motility on bacterial transport in groundwater. *J. Contam. Hydrol* 2004;69:195–213. [PubMed: 15028391]
41. Ford RM, Harvey RW. Role of chemotaxis in the transport of bacteria through saturated porous media. *Adv. Water Res* 2007;30:1608–1617.
42. Cussler, EL. Diffusion: mass transfer in fluid systems. Vol. Second Edition. Cambridge University Press; 1997.

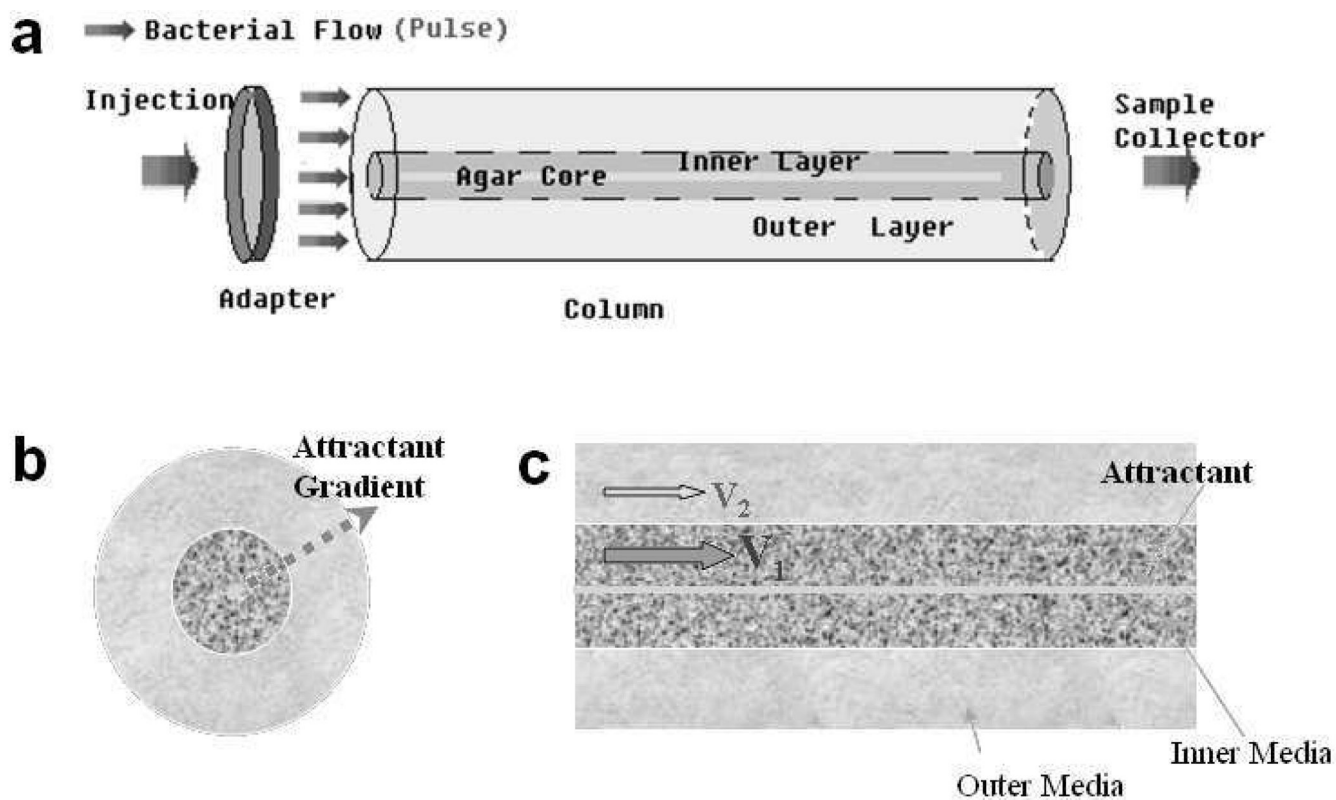


**Figure 1.** Views of the two conductive zones in the structured column: (a) low permeable annulus and high permeable core with an attractant source along the central axis (b) radial cross-section. The attractant is released from the inner source to form an attractant gradient in the radial direction transverse to flow. (c) axial cross-section. Because of the contrasting conductivities in the two layers, the flow velocities in the two layers are also different.

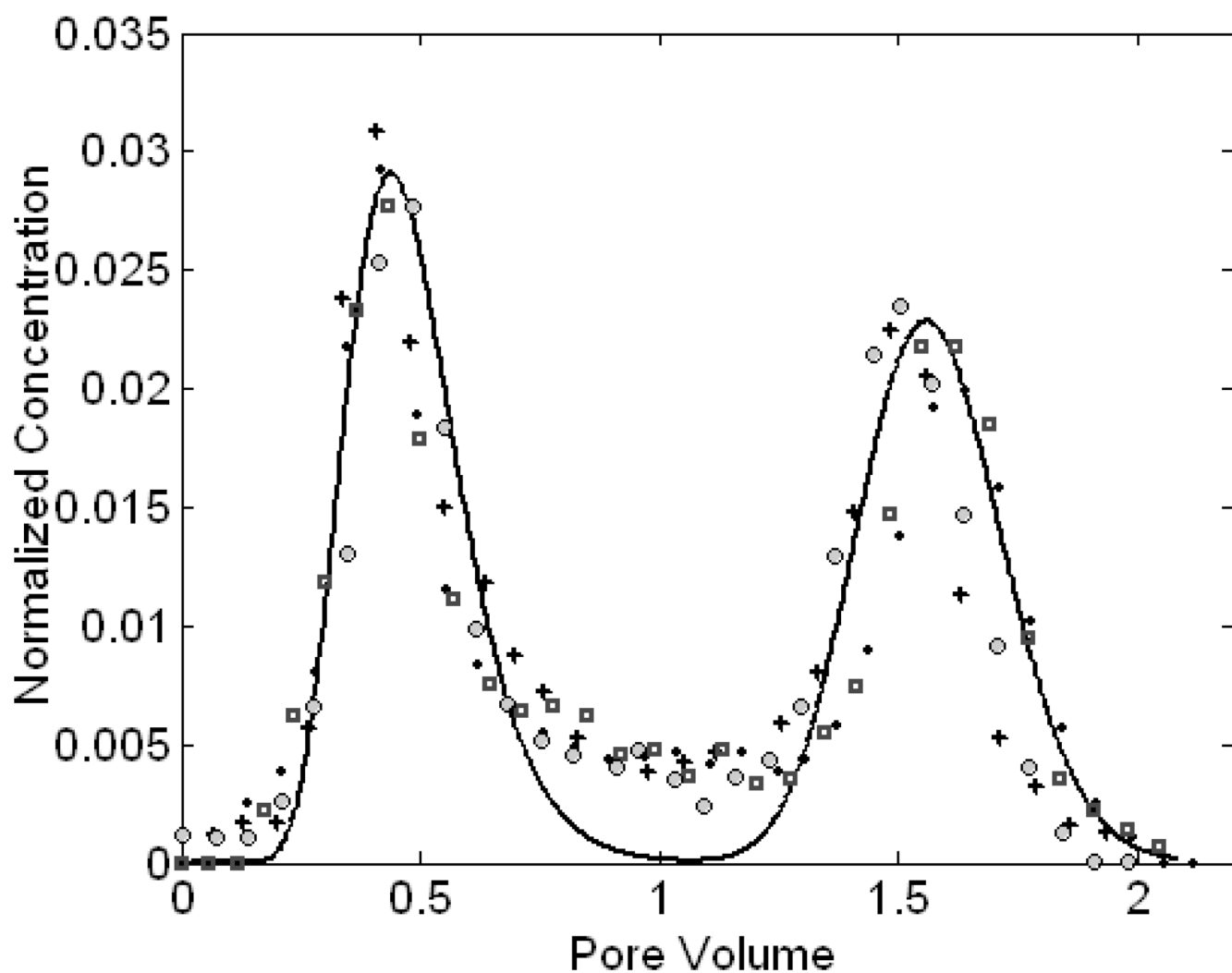


**Figure 2.** BTC of the nitrate tracer at the flow velocity of 5.1 m/d. Nitrate concentrations are normalized to its initial concentration in the injectate. The sparse symbols represent all experimental data from four replicates with different symbols for each replicate and the bold line is the fitted simulated result from the one-dimensional mathematical model using the parameters listed in Table 1.

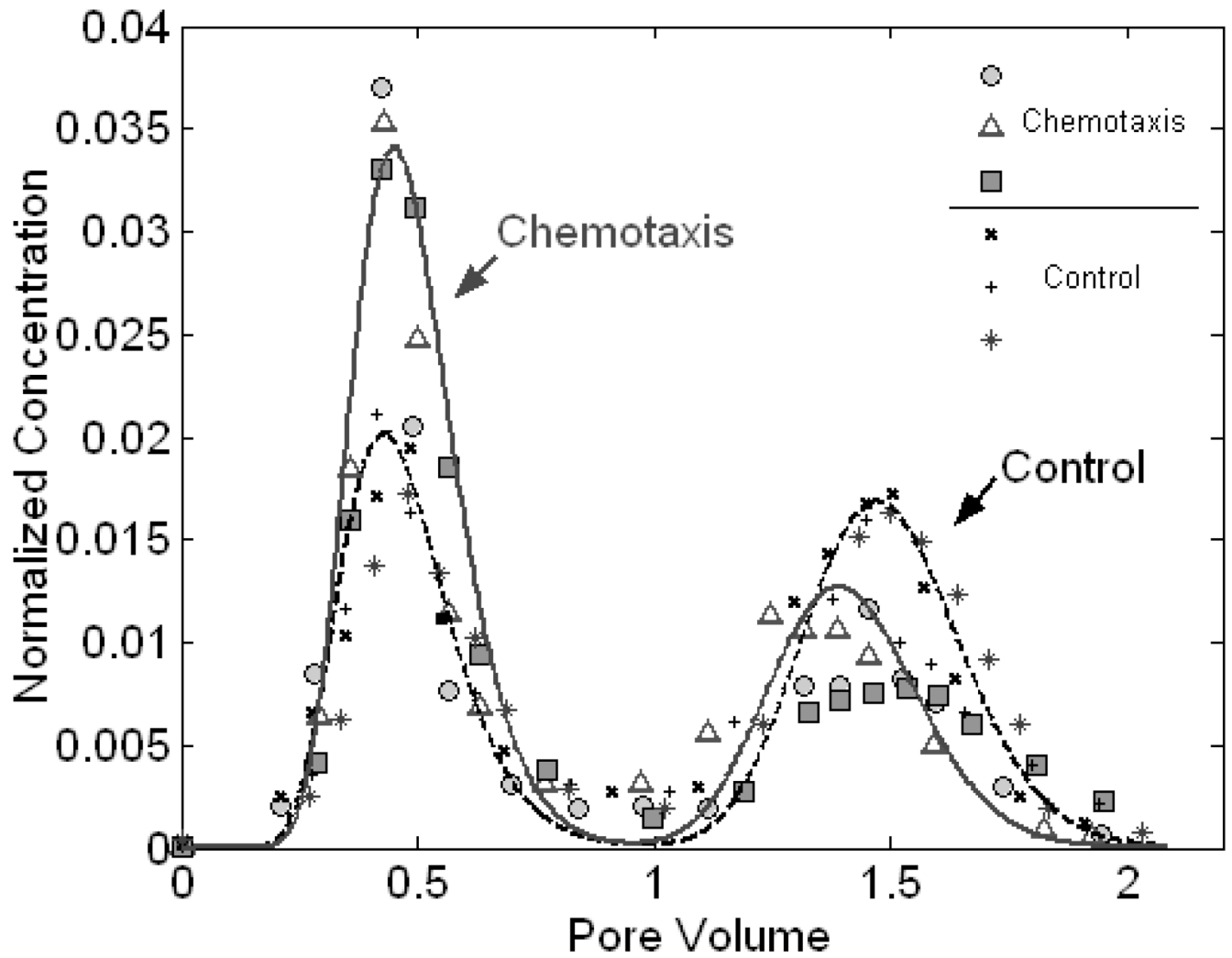


**Figure 3.** BTCs for *E. coli* HCB1 at a flow velocity of 5.1 m/d. Bacterial abundances are normalized to their concentrations in the injectates. Experimental data are shown for both chemotaxis experiments and no-attractant controls, three replicates for each with different symbols as indicated. The simulated results from the one-dimensional mathematical model are represented by the bold line for chemotaxis and the dashed line for no-attractant controls.

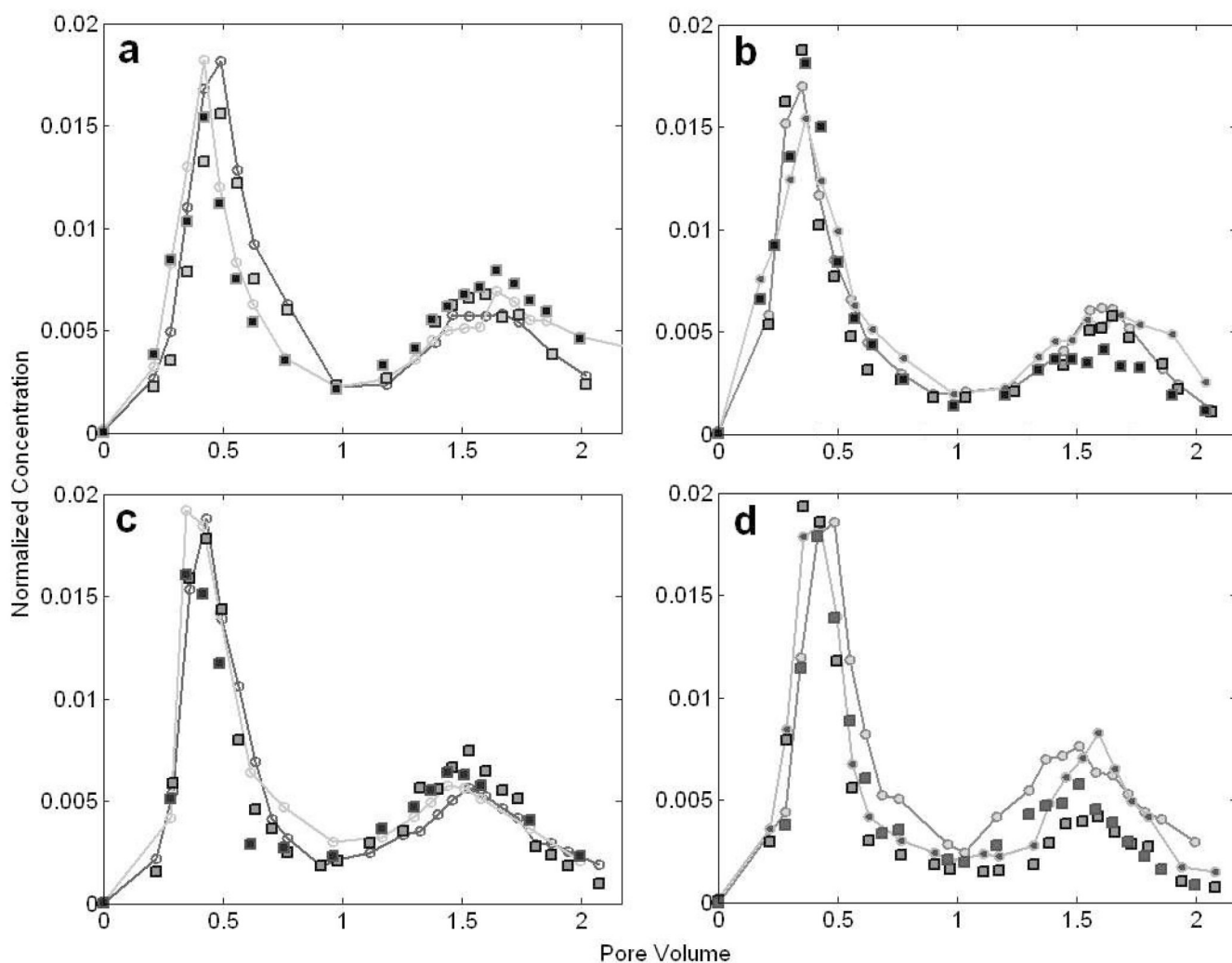


**Figure 4.**

BTCs of *P. putida* F1 at the flow velocity of 5.1 m/d. Bacterial and microsphere abundances are normalized to the initial concentrations in the injectates. The dots connected by lines represent the bacterial data and the squares are for the immobile particles. (a) BTCs of chemotactic bacteria and microspheres for an initial acetate concentration of 0.1 mM. (b) BTCs of nonchemotactic control and microspheres under the same condition as (a). (c) BTCs of chemotactic bacteria and microspheres for an acetate concentration of 1 mM. (d) BTCs of nonchemotactic control and microspheres under the same condition as (c). Data shown are two replicate experiments for each, as indicated by different symbols.



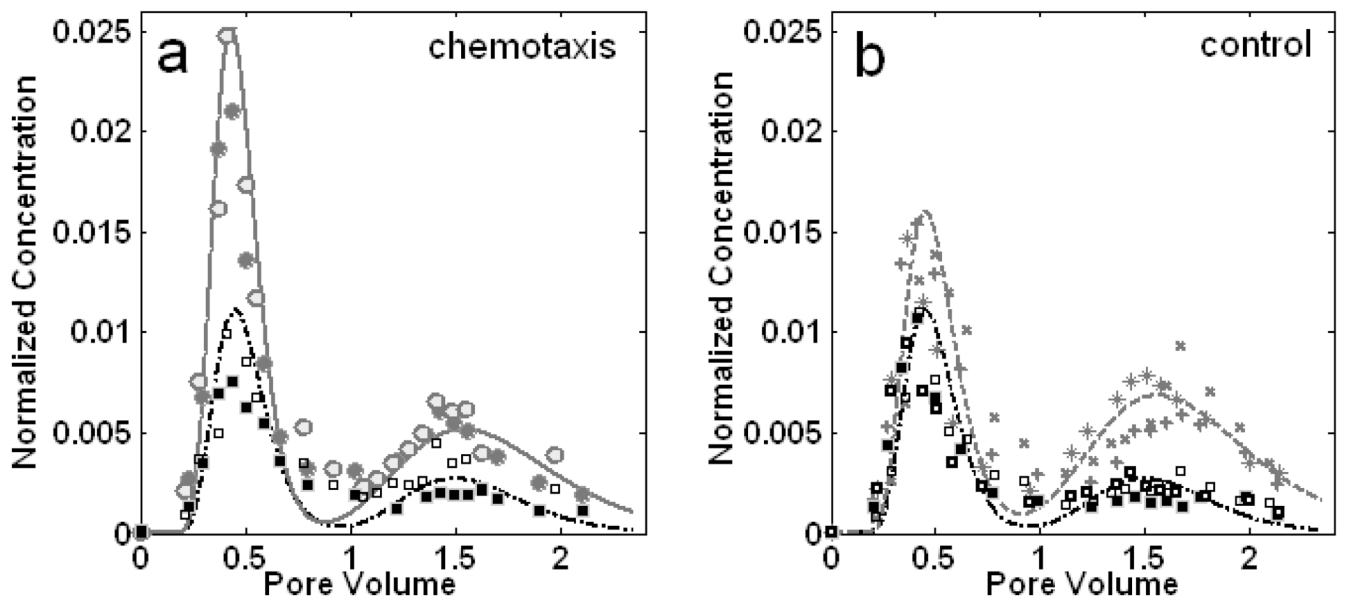


**Figure 5.**

BTCs of *P. putida* F1 and microspheres at the flow velocity of 1.9 m/d. Bacterial and microsphere abundances are normalized to the initial concentrations in the injectates. (a) BTCs of chemotactic bacteria and microspheres for an initial acetate concentration of 0.1 mM. Circles represent chemotactic bacterial data and the bold line is the simulated model. Squares represent microsphere concentration data and the dashed line is the simulated result. (b) BTCs of the nonchemotactic control and microspheres under the same condition as (a) where crosses represent the nonchemotactic bacterial data. Data represents a compilation of two (a) or three (b) replicate experiments, with different symbols representing each replicate.

Table 1

Fitting parameters used in the one-dimensional model for BTCs at 5.1 m/d and 1.9 m/d.

	Coarse Sand Core					Fine Sand Annulus					
	$V_f$ (m/d)	$D_{bc}$ (cm <sup>2</sup> /s)	$\alpha_z$ (m) <sup>a</sup>	$R$	$k_m$ (h <sup>-1</sup> )	$Pe$	$V_f$ (m/d)	$D_{bc}$ (cm <sup>2</sup> /s)	$\alpha_z$ (m) <sup>a</sup>	$R$	$k_m$ (h <sup>-1</sup> )
Tracer	10.9	6.3E-03	2.1E-02	1.00	0.0	1.39E+03	3.3	2.3E-04	1.00	0.0	3.79E+03
Control <i>E.coli</i> HCB1	10.9	6.3E-03	2.1E-02	1.00	1.2	1.39E+03	3.3	3.0E-04	0.95	0.2	2.70E+03
Chemotaxis <i>E.coli</i> HCB1	10.9	4.9E-03	1.6E-02	1.00	-0.2	1.79E+03	3.3	3.0E-04	0.90	0.5	2.70E+03
Tracer	3.5	2.3E-03	2.3E-02	1.00	0.00	4.03E+02	1.2	7.55E-05	1.00	0.00	1.34E+03
Control <i>P.putida</i> F1 Km::CheA	3.5	2.3E-03	2.4E-02	0.93	0.52	4.03E+02	1.2	6.04E-04	1.04	0.08	1.68E+02
Chemotaxis <i>P.putida</i> F1	3.5	1.7E-03	1.7E-02	0.85	0.25	5.37E+02	1.2	6.04E-04	1.04	0.18	1.68E+02
Microspheres	3.5	2.3E-03	2.4E-02	0.95	0.90	4.03E+02	1.2	3.77E-04	1.00	0.48	2.68E+02

<sup>a</sup>Literature values of bacterial motility properties and tracer diffusion characteristics are used to calculate  $\alpha_z$ , including  $\mu_0$  (*E. coli*) =  $3.3 \times 10^{-6}$  cm<sup>2</sup>/s (35),  $\mu_0$  (*P. putida*) =  $1.3 \times 10^{-6}$  cm<sup>2</sup>/s (21),  $\mu_0$  (microspheres) =  $2.0 \times 10^{-9}$  cm<sup>2</sup>/s (41),  $\mu_0$  (tracer) =  $1.9 \times 10^{-5}$  cm<sup>2</sup>/s at 25°C (42), and  $\tau = 1$  (18).